International Journal of Applied Glass Science, 1–14 (2015)
DOI:10.1111/ijag.12133

INTERNATIONAL JOURNAL OF
Applied Glass
SCIENCE

Crack and Shock Propagation through the Interlayer in Soda lime Glass under Detonation Loading

Joon Hong Choi

Department of Materials Science and Engineering, Korea Advanced Institute of Science and Technology (KAIST), 291 Daehak-ro, Yuseong-gu, Daejeon 305-701, Korea

The 5th R&D Center, Agency for Defense Development, P.O.Box 35, Yuseong-gu, Daejeon, 305-600, Korea

Do Kyung Kim*

Department of Materials Science and Engineering, Korea Advanced Institute of Science and Technology (KAIST), 291 Daehak-ro, Yuseong-gu, Daejeon 305-701, Korea

Dynamic wave interaction and crack propagation in glass have been observed with the edge-on impact (EOI) style test method using an exploding bridged wire (EBW) detonator. The existence of an interlayer or internal surface displayed meaningful wave distortions, delays, reflections, and decreasing amplitude. The interlayer materials used were rubber, stainless steel, and cut surface. The results indicate that the shocks passing the interlayer decrease following the impedance condition and that much of the crack is stopped at the interlayer. The damage pattern was analyzed with the energy and stress dissipation rate.

Introduction

When an intense shock is loaded onto the surface of a material, it experiences a severe energy dump and acts to dissipate this energy through various mechanisms, such as physical, mechanical, or even chemical reactions. Shock interaction is a very important field in the research of protection mechanisms and armor design. The huge shock energy generated by a ballistic impact creates high stress on the material and causes severe elastic/plastic deformation and/or increased temperature. The majority of modern armor does not use one type of material but a combination of various materials to overcome the various types of threats. Recently, brittle nonmetallic materials such as ceramic and glass have been widely used to reduce weight and increase ballistic performance.[1,2] Many researchers have studied the mechanism of material response when the material is subjected to a large shock or ballistic impact using impact experiments and numerical analysis.[3–6]

Shockey *et al.*[7] researched detailed ceramic fracture phenomena by impacting a long-rod penetrator and a tungsten carbide sphere. The impact was investigated

*dkkim@kaist.ac.kr

after impact occurred by postmortem technology. Shin *et al.* also revealed a bulk metallic glass fracture with an explosive detonation impact by this same postmortem technique.[8] They performed an explosive indentation test using a small EBW (explosive bridged wire) detonator. Because the majority of armor ceramics are opaque, it is difficult to investigate their real dynamic responses *in situ* by light transmission. For ceramic, such as SiC, the side faces were polished to a mirror-like finish so that cracks in the surface were observed by reflected light.[9] Flash X-ray is a useful instrument in which the X-ray penetrates low-density brittle material and creates an image of the material state.[10,11] This technology is well known. However, the resolution and the required number of images limit the ability to acquire good information in the dynamic impact process. Because of the rise in local conflicts worldwide, the importance of transparent armor has increased. Traditionally, glass laminated with a polymer film has been the typical material used to cope with a ballistic threat. To improve performance, transparent plastic or ceramic is considered. The key is to reduce weight and thickness. Good candidates for improved performance are sapphire, AlON, and some glass ceramics. Researchers have studied the characteristics of these materials in the static and dynamic state, as well as during ballistic impact.[12–14]

Previous studies on various transparent materials for dynamic impact were performed using a method called the "edge-on impact" (EOI) method.[15] When a projectile with a hemispheric, flat or sharply pointed nose shape impacts a specimen, it generates an intense shock, fragments the specimen and penetrates it. As the energy delivery rate to the specimen depends on the geometric shape of the projectile head, the propagating wave and crack are also affected and distorted. To minimize these effects, we considered a detonator that can load a shock pulse as a point-like source without massive penetration.

In this study, we investigated the dynamic fracture behavior of glass in relation to the boundary condition and shock response under intense loading with a small explosive detonator. The effect of the interlayer and interface in the material on the crack growth and shock wave interaction was well visualized and analyzed. This study demonstrates that acoustic impedance is an important factor for wave interaction at the interface and that it affects crack growth and propagation.

Experimental Procedure

Material

Glass material was supplied as a plate and cut to specimen size. To sustain good transparency, observation surfaces were polished, and contact interfaces were lapped and polished to below 0.6 μm surface quality to secure good contact conditions. A bulk specimen that has no interlayer has a size of 50 × 50 × 11 mm^3. The specimens that include an interlayer consist of two glass plates of 50 × 25 × 11 mm^3 and the interlayer material. Selected glass and interlayer materials used in the experiments are displayed in Table I.[16] The symbols in Table I are denoted as density ρ, elastic modulus E, Poisson's ratio ν, longitudinal sound speed C_L, and shear wave speed C_S. The interlayer material was squeezed in between two glass plates. The compositions of the soda lime glasses are given in weight percent in Table II.[16]

Exploding Bridged Wire (EBW) Impact

EBW is a detonator used to trigger mass explosion in defense research. The model used here is RP-87, a commercial model of Reynolds Industries that contains an output explosive of 43 mg RDX with 26 mg PETN for initiating explosion in a 152.4-μm-thick stainless steel case.[17] The value of the shock pressure can be easily determined with simple calculations. The Gurney energy for the open-faced sandwich is indicated in Eq. (1),[18] where M is the total metal mass (21.88 mg), C is the total explosive mass (69 mg), v is the metal velocity, and $\sqrt{2E}$ is the Gurney energy (2.93 ㎜/μs). For the EBW, the metal velocity (v) is calculated as having a value of 2.94 km/s.

Table I. Physical Properties of Soda Lime Glass and Selected Interlayer Materials

	ρ(g/cm^3)	E (GPa)	ν	C_L (km/s)	C_S (km/s)
Soda lime glass[16]	2.50	73	0.23	5.59	3.40
Stainless steel	7.80	210	0.28	5.77	–
NBR rubber	1.0	–	–	1.60	–

Table II. Soda Lime Glass Chemical Composition (wt%)[16]

SiO_2	Na_2O	CaO	MgO	Al_2O_3	K_2O	SO_3	Fe_2O_3
72.70	13.00	8.80	4.30	0.60	0.40	0.20	0.02

$$\frac{v}{\sqrt{2E}} = \left[\frac{\left(1+2\frac{M}{C}\right)^3+1}{6\left(1+\frac{M}{C}\right)} + \frac{M}{C}\right]^{-\frac{1}{2}} \quad (1)$$

In addition, we can assess loading stress by the graphical method, applying the available EOS data from LASL Shock Hugoniot.[19] When a stainless steel plate (EBW cup) impacts the Pyrex plate (target) at a velocity of 2.94 km/s, the contact interface has a velocity of 2.30 km/s, and the value of the shock pressure can be calculated as 27.7 GPa (Fig. 1). The calculated value is compared to the particle velocity of real detonation loaded onto the glass plate, which was measured with the velocity interferometer system for any reflector (VISAR). The maximum interface velocity was 2.3 km/s at 1.2 μs after the explosion, and this correlated well with the value from the graphical solution.[20] The test material used in the experiment was soda lime glass. It has a density ~10% higher than that of Pyrex (ρ = 2.20 g/cm^3) and a similar longitudinal sound velocity ($C_{L,\ Pyrex}$ = 5.56 km/s, $C_{L,\ Soda}$ = 5.59 km/s).[19] When we considered the composition and the sound velocity of Pyrex versus soda lime glass, the Hugoniot stress generated on the impact surface of soda lime glass was expected to be slightly higher than that of Pyrex.

Experimental Configuration

A specimen setting configuration with an EBW is displayed in Fig. 2. For a tight contact effect, two glass plates and interlayer materials were confined with four steel blocks, and each block was screwed to the other block. An EBW was inserted into the hole on the top block and glued for a secure fixation. The contact surfaces of each steel block that contact a glass specimen were machined to be flat to secure impedance matching.

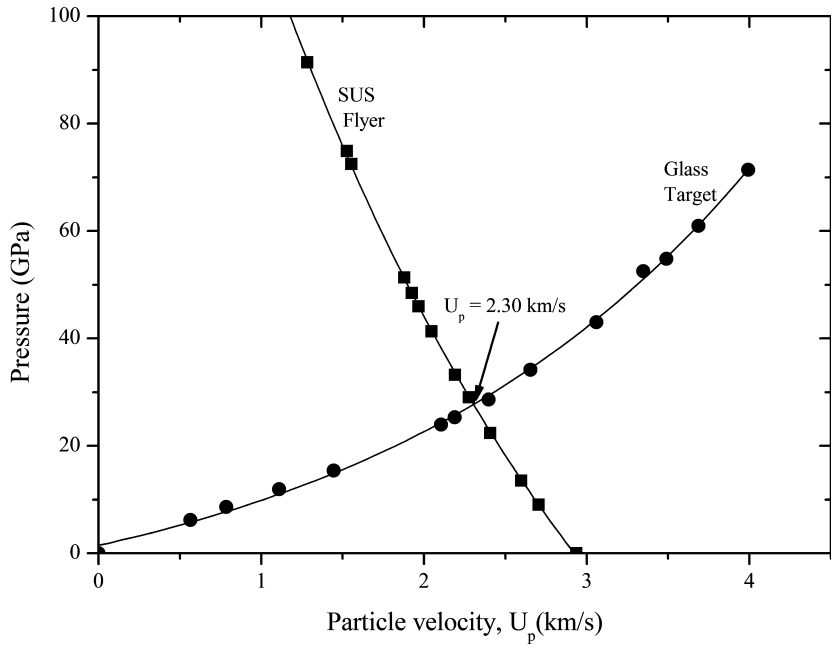

Fig. 1. Graphical solution for plate impact experiment when a SUS flyer impacted a Pyrex glass target with the speed of 2.94 km/s.

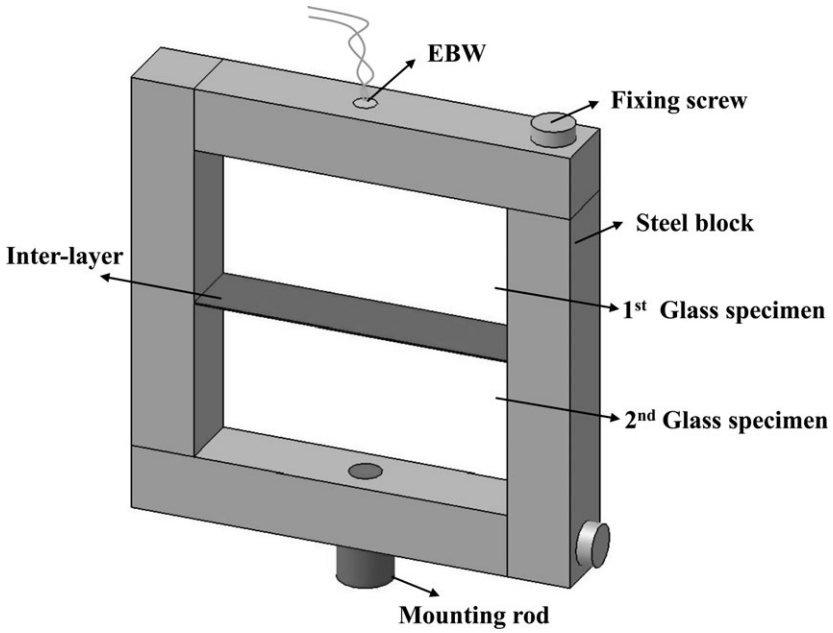

Fig. 2. Configuration of specimen setting with an EBW.

Figure 3 displays the experimental setup. An experimental tank made of steel boxes ($60 \times 60 \times 60$ cm^3) with two observation windows was used for protection from fragment debris. Due to the very short time duration of the shock propagation and crack generation, a precise trigger method is essential. A Fresnel lens was used to provide parallel light illumination from a point source. The parallel light passed through the specimen, reached the camera, and produced a shadow photograph of the specimen's status in real time. The ultra-high-speed imaging system (Specialised Imaging Limited, SIMD16) can produce 16 photographs at up to 2 billion frames per second. A delay generator can control the equipment at a designated trigger time with microsecond time resolution.

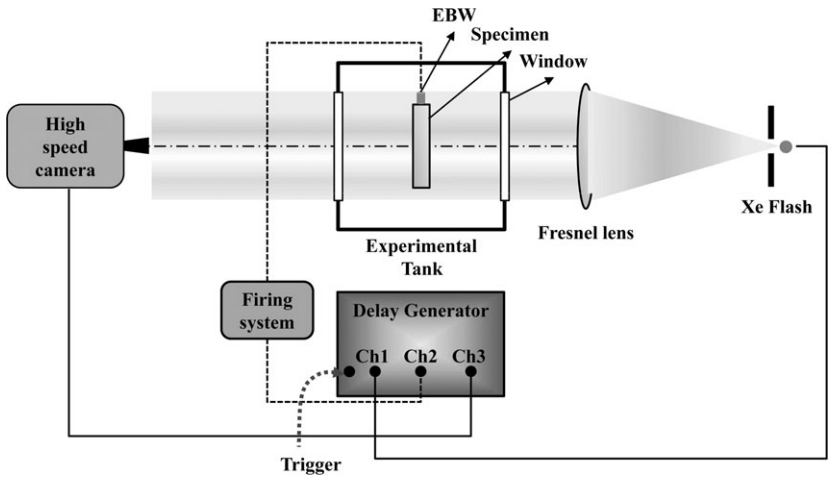

Fig. 3. Experimental setup for high-speed photography.

Shock Wave Interaction at the Interlayer

The interface has a discontinuity of material characteristics, resulting in a shock wave that is greatly influenced by those boundary conditions. The existence of the interlayer provides an interesting wave reaction at the interface and also provides a hint to reduce fragmentation or attenuate shock strength. Shock wave transmission and reflection behavior in the material is well described by M. A. Meyers.[21] When a shock wave propagates from material **A** to **B**, the stress wave relation of incidence (σ_I), reflection (σ_R) and transmission (σ_T) at the interface is denoted as Eq. (2). Thus, the acoustic impedances of materials **A** ($\rho_A C_A$) and **B** ($\rho_B C_B$) have great importance in deciding wave character, where the density and sound wave speed are ρ_A, C_A, ρ_B, and C_B, respectively.

$$\frac{\sigma_T}{\sigma_T} = \frac{2\rho_B C_B}{\rho_B C_B + \rho_A C_A}, \frac{\sigma_R}{\sigma_I} = \frac{\rho_B C_B - \rho_A C_A}{\rho_B C_B + \rho_A C_A} \quad (2)$$

Results and Discussion

Damage of Glass Laminates with Mechanical Contact

Glass laminate, which consists of two glass sheets, was contacted with just the confining steel blocks. It was softly squeezed to ensure a mechanical contact that gave an acoustic impedance matching condition. Four setting screws were used to remove air gaps at the contact surface. Figure 4 displays the series of high-speed photographs and propagation characteristics of the wave and damages following the analysis of Straßburger *et al.*[12,22] The shock wave generated from the impact point exhibits a spherical shape and propagates with a speed of 5.95 ± 0.09 km/s in the first glass specimen. From the interface, part of the wave is reflected with a speed of 5.85 ± 0.11 km/s, and the residual stress wave passes through the interface with a speed of 5.83 ± 0.11 km/s. The measured velocities from the photographs are somewhat higher than that of longitudinal sound speed. As the two consecutive materials at the interface are the same, the incident stress wave is expected to pass the interface without reflection. However, a considerable part of the wave is reflected from the interface and back into the impact point. The mechanism of this unexpected result is not yet known precisely. Although both contact surfaces were polished below the submicron level, the microstructure of both surfaces could not match completely. For a detailed description, micro-structural treatment of the surface would be required. This remains to be studied in future work.

The damage pattern is similar to those in other investigations with borosilicate glass.[11,22,23] After 5.6 μs of impact, a few cracks begin to nucleate in the direction of the impact point at the interface, gradually grow, and finally integrate as large damage. This backward fracture (▽) in Fig. 4b seems to resist forward fracture (△) propagation of the main fracture front in the 1st glass. At 9.6 μs, both fractures meet and do not exhibit any considerable expansion thereafter in high-speed photographs. However, the post-test photograph (shown in Fig. 10a) displays damage passing through the interface. Thus, the fracture generated at the interface (and moving backwards) at approximately 7.6 μs is the result of tensile stresses generated by reflection at the interface.

Fracture shapes are different with different loading rate and the shapes of the impactor. With an EBW detonator indentation, we can clearly observe a Rayleigh cone at the initial time of impact. Because the specimen is sufficiently small, the Rayleigh cone shape is integrated with the fracture front damage. The amplitude of the shock waves in the material decays as r^{-1}, but it decays as r^{-2} along the surface. On the impact surface, the Rayleigh wave is dominant, but the compression and shear waves are dominant in the inner part of material. Thus, the damage shape is governed initially by the characteristics of the Rayleigh wave. Later, it is affected by the compression and shear waves. Figure 5 displays a Rayleigh cone at 3.6 μs after an EBW detonation loading, and the cone angle is measured to be approximately 22°. The calculated Rayleigh wave speed (C_R) of the soda lime glass according to Eq. (3)[21,24] is 3.11 km/s, where v is the Poisson's ratio and C_S and C_L are the shear and longitudinal wave speeds.

$$C_R = \frac{0.87 + 1.12v}{1 + v} C_S, C_S = C_L \sqrt{\frac{1 - 2v}{2(1 - v)}} \quad (3)$$

Yavari and coworkers[25] investigated the terminal velocity of rough cracks on a theoretical basis. The Rayleigh wave speed calculated from their work is almost the same as the result with Eq. (3). In addition,

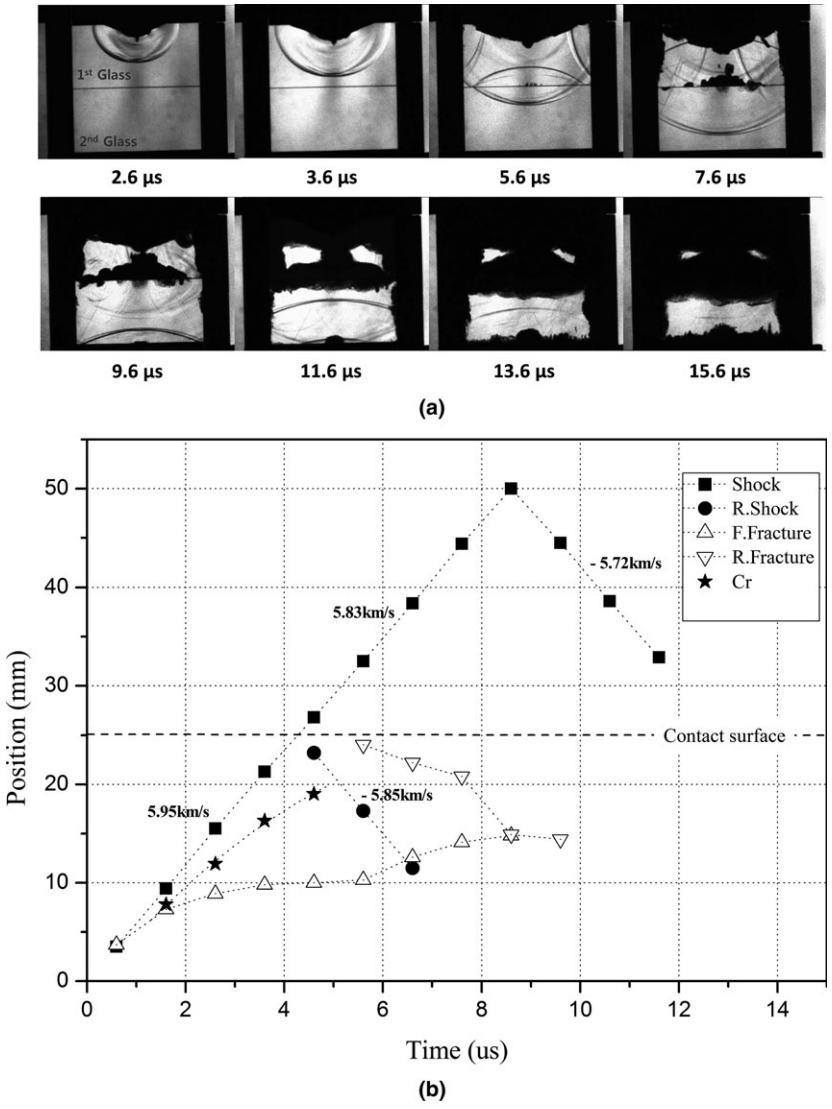

Fig. 4. Analysis of contact specimen. (a) Selected high-speed photographs of the glass laminate of the horizontal contact. (b) Fracture and wave propagation with time sequence.

the predicted terminal crack velocity of glass (ν = 0.22) is denoted as $0.32C_L$ and is in the range of $0.28C_L$–$0.39C_L$ for the experiments. From the pictures taken at 2.6 μs and 3.6 μs in Fig. 4, the velocity of the circular crack front [(V_C), which is defined in Fig. 5] is measured as 1.51 km/s. This is somewhat lower than the predicted value ($0.32C_L$ = 1.8 km/s) but is similar to the lower experimental value ($0.28C_L$ = 1.57 km/s). Kanel and coworkers[26] indicated that the failure wave speed of soda lime glass was 1.58 km/s at the compression stress of 6.3 GPa with the plate impact experiment. Therefore, the crack velocity in the forward direction at the initial state is similar to the failure velocity and limit crack velocity as investigated by others. Anderson and coworkers[24] studied the crack and damage velocities of a borosilicate in ballistic experiments. They measured the crack velocity for Borofloat 33 (ν = 0.20) as 1.92 km/s and evaluated it with

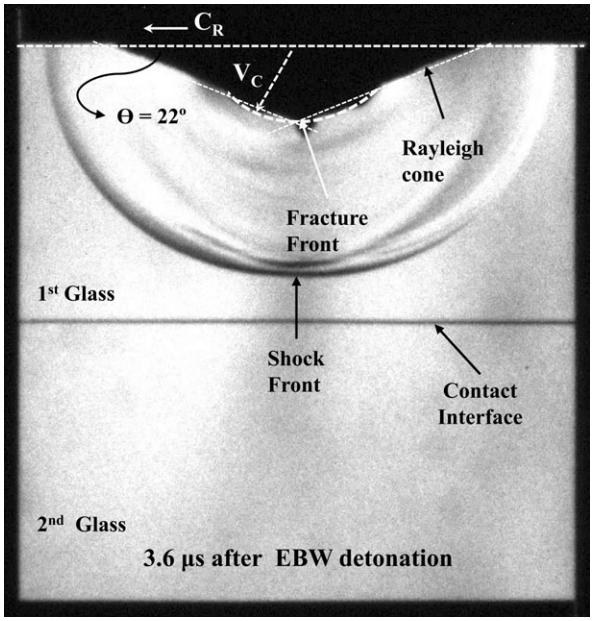

Fig. 5. Configuration of crack and wave propagation at 3.6 μs after EBW detonation.

the Rayleigh wave relation, Eq. (3). The predicted velocities of the crack are in the range of 0.5~0.6 times the Rayleigh wave speed.

Brajer *et al.*[27] determined the Rayleigh cone angle (θ) using the relation in Eq. (4). They used a speed C_R on the order of 3.3 km/s and a V_C value of 1.5 km/s and assessed the theoretical angle to be 28°. However, in our experiments, the surface crack on the impact surface (★) is observed to propagate faster than the Rayleigh wave. The measured speed of the crack, which follows the path of the Rayleigh wave propagation in the time interval between 2.6 μs and 3.6 μs, is 4.54 km/s, even though the calculated speed of the Rayleigh wave is 3.11 km/s. When a C_R of 3.11 km/s and a V_C of 1.51 km/s are used, θ is calculated as 29°. When the crack velocity measured in the experiments, 4.54 km/s, is inserted into Eq. (4), θ is calculated to be 19.4°, which is in better agreement with the experimental results than the theoretical calculation. The measured cone angles from the experiments are 22° for the confined specimen shown in Fig. 5 and 19.5° for the specimen with a free surface. When we consider those angles in relation with Eq. (4), this reveals that the crack grown on the free surface grew faster than that on the surface confined with steel blocks.

$$sin\theta = \frac{V_C}{C_R} \tag{4}$$

The Rayleigh cone is generated by the tensile stress wavelets that are formed with the interaction of the longitudinal wave with the impact surface.[21] Abraham and coworkers[28] studied brittle crack propagation by two-dimensional molecular dynamic simulation. They indicated that mode I (tensile) crack was quickly accelerated but was limited to the Rayleigh wave speed, consistent with the classical theories of fracture. The mode II (shear dominated) crack first accelerated to the Rayleigh wave speed, propagated at the Rayleigh speed for a while and then jumped to the longitudinal sound speed. Thus, the cause of the crack on the impact surface of EBW loading is considered to be a mixture of tensile and shear stress because the initial crack on the impact surface grew faster than the speed of the shear wave and propagated slowly later with the loss of energy.

Consideration of Acoustic Impedance

Table III displays the acoustic impedance of materials used in the experiment. Rubber has a very low value compared to glass. Although stainless steel has a similar sound speed, the value of acoustic impedance is three times higher than that of glass because the density is that much higher. Applying Eq. (2) for shock wave interaction, the amplitude of transmitted stress is $\sigma_T = 0.20\sigma_I$ and that of reflected stress is $\sigma_R = -0.80\sigma_I$ at the glass and NBR rubber interface. This means that the majority of the initial stress is reflected as tension at the interface, and only 20% of the input stress is transmitted. Thus, the shock wave

Table III. Acoustic Impedance of Selected Materials

Material	Density (ρ) (g/cm^3)	Sound speed (C) (km/s)	Acoustic impedance (10^6 kg/m^2s)
Soda lime glass	2.50	5.60	14.00
NBR rubber	1.00	1.60	1.60
Stainless steel	7.80	5.77	45.03

intensity (in Fig. 6) that passed through rubber is clearly demonstrated to be dimmer than that in Fig. 4. The fracture cannot progress through the NBR rubber. This indicates that the shock amplitude and fracture generation at the boundary should be reduced.

For the specimen that has a glass and SUS interface, the amplitude of transmitted stress calculated is $\sigma_T = 1.52\sigma_I$ and that of reflected stress is $\sigma_T = 0.52\sigma_I$. By simple calculation using the impedance relation, the expected amplitude of stress in the second soda lime glass is $\sigma_T = 0.36\sigma_I$ for the NBR rubber interlayer and is $\sigma_T = 0.73\sigma_I$ for the SUS interlayer, as seen in Fig. 7. Thus, NBR rubber is a more effective material as an interlayer to reduce stress amplitude than SUS. From Figs 6 and 8, we deduced the above shock relation and found some important information for boundary design to reduce fracture at the interface.

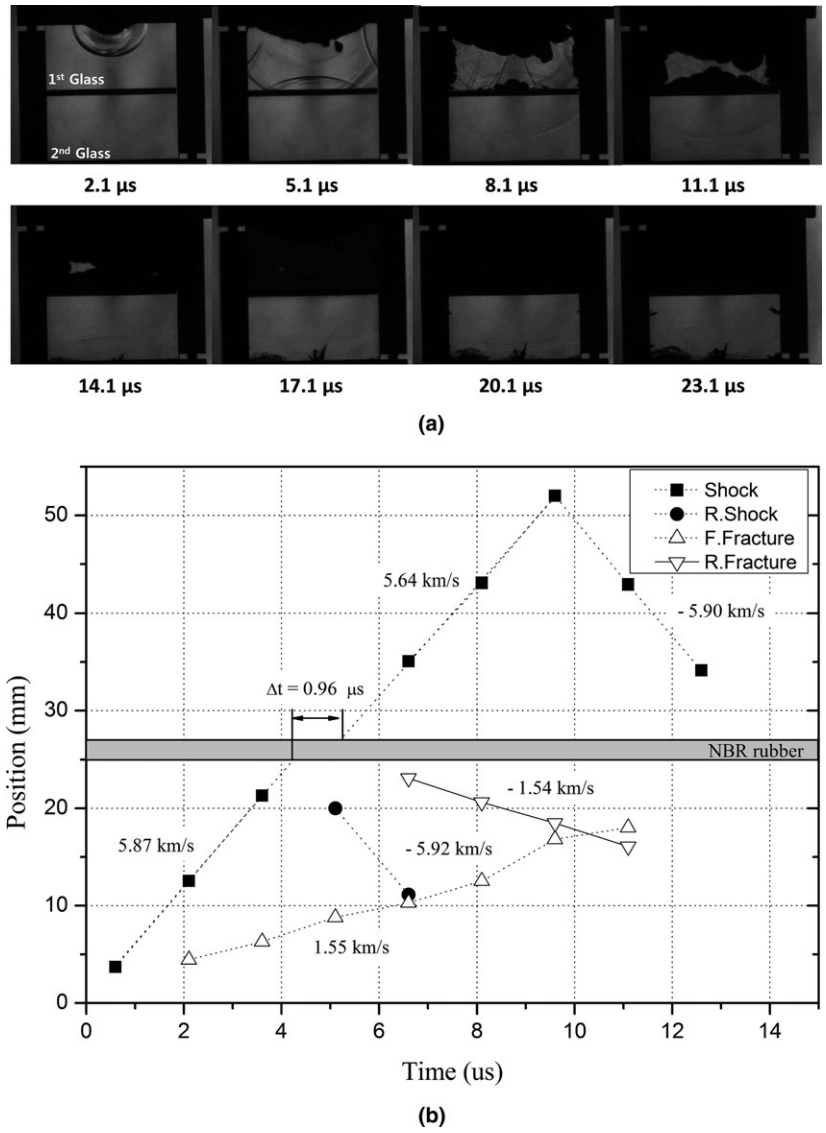

Fig. 6. Analysis of interlayered specimen. (a) Selected high-speed photographs of the glass laminate with NBR rubber interlayer. (b) Fracture and wave propagation with time sequence.

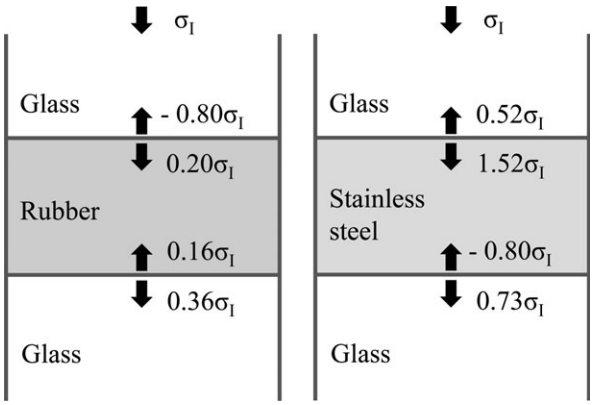

Fig. 7. Stress wave intensity relation at interfaces with simple calculation applying the acoustic impedance of Table III.

Damage of Glass Laminates with NBR Rubber Interlayer

In this experiment, a low-impedance material was inserted in between relatively high-impedance materials. Due to the low impedance of rubber, there are considerable stress wave attenuations, distortions, and reflections. Figure 6 displays a series of high-speed photographs and wave/fracture locations with respect to time sequence. As wave delay and attenuation were expected to occur, the framing time rate of the camera was changed to 1.5 μs/frame. The shock wave (■) propagates at an initial speed of 5.87 ± 0.02 km/s in the glass, reduces its speed to 2.08 km/s in the NBR rubber, and recovers its speed in the second glass. However, the shock speed is decreased to ~4%, and its intensity seems to be lower than that of the first glass because the transmitted wave is observed to be considerably dimmer in the second glass than in the first glass. There is a discontinuity found in Fig. 6b for the shock propagation data. Although shock wave speed seems to be somewhat decreased after passing through the interlayer, it does not depart from the linearity except for time delay $\Delta t \approx 0.96$ μs. Comparing Fig. 6 with Fig. 4, the shock wave passing through the interlayer appears dimmer than that of the bulk specimen at the same propagation distance. The horn-shape crack that nucleated and grew at the bottom center from 14.1 μs is due to tension concentration at a hole for the M6 screw used to fix the steel block for mechanical mounting. The fracture growing speed from the impact surface to the interlayer (Δ) is nearly the same as that from the interlayer to the impact point (∇).

Damage of Glass Laminates with Stainless Steel Interlayer

The stainless steel interlayer plate has a dimension of 50 × 11 × 2 mm^3. The acoustic impedance of the SUS is three times higher than that of glass, so the wave interaction at the interlayer was expected to be different from those of the other results. The measured shock wave speed (■) is 5.98 ± 0.15 km/s. In Fig. 8a, the fracture in the first glass plate was mainly generated after the reflection of stress waves at the edge of specimens, as the Starphire glass demonstrates.[29] However, the second glass does not exhibit many cracks, except for the central bottom region, which was contacted with a threaded vacant hole for fixing blocks to the magnetic base.

Figure 8b displays the positions of the wave and fracture tip. Wave propagation and reflection speed do not change significantly considering measurement errors, with the exception of the second reflected wave (▲), which is reflected after passing through the stainless steel plate. The fracture front speed (△) from the impact surface to the bottom is changeable with the existence of flaws inside or on the surface and is estimated to be in the speed range of 0.57 km/s to 2.01 km/s. However, the fracture generated from the stainless steel plate to the impact surface is considered to be due mainly to tension, and the fracture propagation speed is approximately 1.38 km/s in each frame. It is interesting that the fracture due to the shock wave relation does not transfer actively to the next neighboring specimen, as the specimen with rubber was used as an interlayer.

Energy Dissipation

Haney and Subhash showed that the elastic shock wave consumed more than one third of the impact energy in Spinel and sapphire.[29] In this work, we assessed the energy dissipation of the specimen with simple calculations and compared the results with that of the numerical results of pressure distribution. The initial energy density generated by the wave is $w_0 = \sigma\varepsilon$. The energy dissipation density in the wave field is given by $w(r) = \frac{dW}{dV}$, where $V(r)$ is the volume that the wave front swept, and r is a distance from the impact point.[30] From this experimental geometry, the energy density is given as $w(r) = \frac{w_0 A_0}{\pi r d}$, where A_0 is the impact area, and d is the target thickness. When we considered

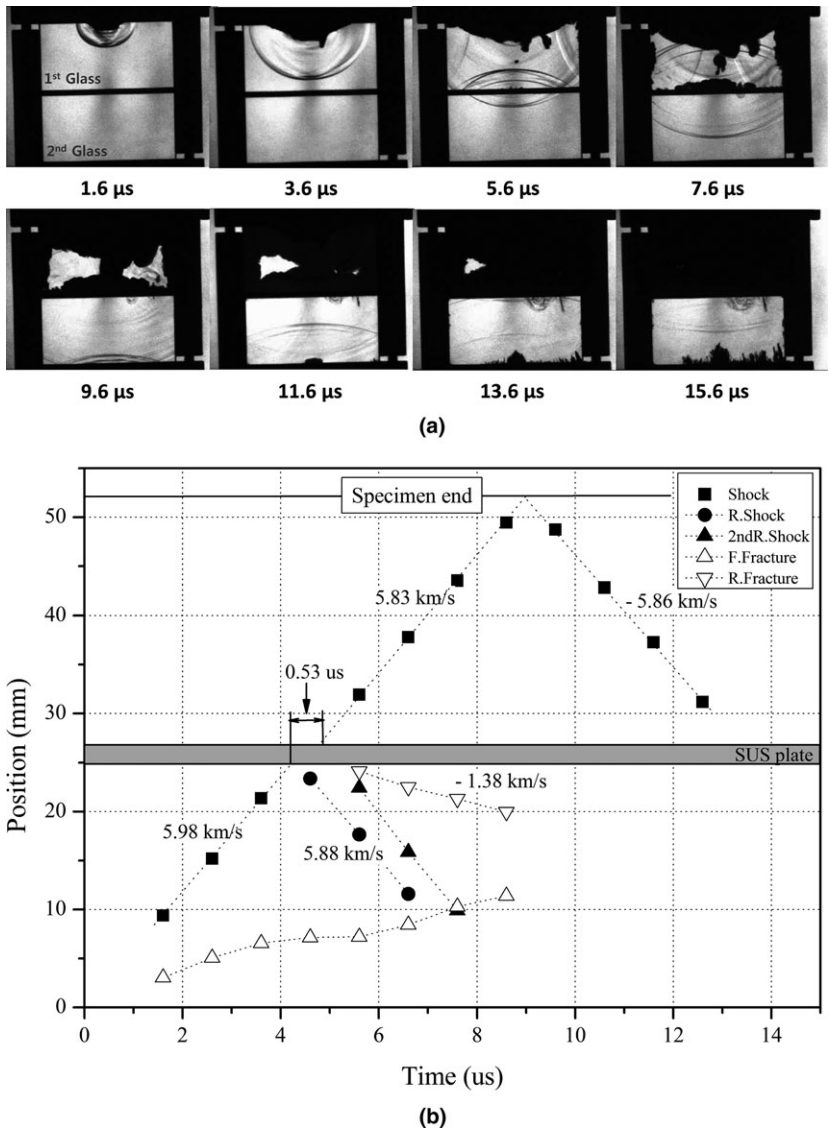

Fig. 8. Analysis of interlayered specimen. (a) Selected high-speed photographs of the glass laminate with stainless steel interlayer. (b) Fracture and wave propagation with time sequence.

that the effective EBW impact diameter is 4.5 mm and target size is $50 \times 50 \times 11$ mm^3, A_0 is 6.35×10^{-5} m^2 and d is 0.011 m. With a simple calculation, we can see that the energy density curve displays an r^{-1} slope. The impact surface is so small that a rapid attenuation of energy density is expected.

In a real case, the shock strength is considered to be attenuated with propagation distance, time, and material characteristics. Thus, the stress expectation amplitude at any position is somewhat different. With numerical analysis, stress attenuation can be assessed with respect to distance and time when the numbers of the pressure gauge are imbedded inside of the material.[31] Numerical analysis was performed on the configuration (Fig. 9a) by using the material data available in the AUTODYN library. Damage, shock wave propagation, and pressure distribution in the material were calculated in the sequence of time. The normalized

pressure at each location is defined as the value [value of the pressure at location (r)/value of pressure at the impact point ($r = 0$)]. The normalized energy density also can be described with the same manner. The pressure attenuation and energy dissipation with distance from the impact point are displayed in Fig. 9b. Grady[32] has modeled a spherical shape stress pulse (σ) as a function of the distance from the impact point and time in the form

$$\sigma(r, t) = \sigma_0 r^{-\frac{1}{2}} e^{-\frac{t}{\tau(r)}} \tag{5}$$

where, σ_0 is an initial stress, r is the distance, and $\tau(r)$ is the elastic constant. The failure region is expected to

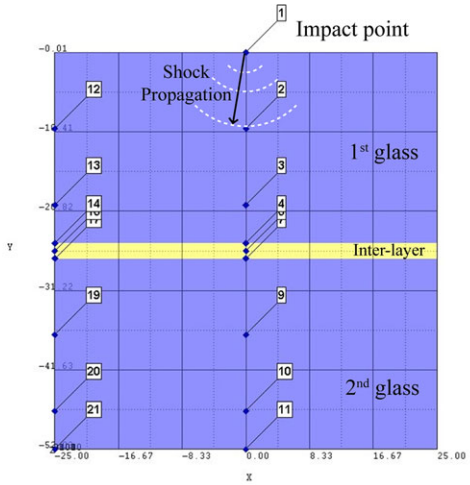

Fig. 9. Energy and pressure dissipation. (a) Pressure calculation model with implanted gauge. (b) Normalized energy density and pressures at each gage location.

be bounded within a certain region from the impact point because stress strength decreased with time and distance, and eventually, sufficient energy is not provided to grow the crack. When we apply the numerical analysis results to Eq. (5), the elastic constant (τ) is assessed with respect to the propagation distance and time. It is 1.11×10^{-5} at 10 mm and varies from 3.19×10^{-6} at 20 mm to 3.44×10^{-6} at the bottom surface.

Figure 9b displays the rate change of the energy density and stress with the propagation distance (r). For the contact specimen (■), stress is attenuated with a pattern similar to the energy curve (□). The pressure rate change in the interlayer is different from that in the homogeneous block due to impedance mismatch. For an interlayer material of higher impedance than glass, the stress shows a higher value than that of adjacent glass (▲). For the NBR interlayer, the stress value decreases abruptly (◆) compared with the stress of the homogeneous block (■). These results match the impedance relations in Fig. 7 and fracture patterns observed in-situ and postmortem. For the point impact used in this study, the impact energy dissipation results in an increase of volume that is matched to the fracture configuration.

Damage Analysis

Figure 10 displays the damage configuration of the recovered specimen. Although the same impact energy is delivered to specimens, we can clearly observe the effect of the interlayer as expected. Underneath the impact point, the comminuted zone is well identified. However, fracture particles become bigger than the particles of the impact point as the distance from the impact increases. In addition, the damage patterns of the glass specimen on the interlayer or boundary are quite different from the damage pattern of the internal material. From all specimens, fine comminuted particles are generated on the contact surface due to tension caused by the reflection of the stress wave on the surface. Straßburger and coworkers[12] investigated wave and damage propagation in Starphire glass laminates with cylindrical projectile impact. They used a polyurethane (PU) bonding layer as the interlayer material and examined the influence of interlayer thickness. With increasing PU thickness, it was observed that damage in the second specimen was considerably reduced. Park[33], Parab, and Chen[34] investigated the dynamic crack propagation across a perpendicular interface in a glass specimen with the shape of notched edges. Single crack propagation phenomena through an interface with or without adhesive were analyzed by impact experiments. With an impact velocity of below 300 m/s, a single crack was generated at the notch and propagated to the next layer. They found that a crack that was an opening mode (Mode I) stopped at the interface where two glass plates were simply contacted without adhesive. However, stress waves transferred to the adhesive effectively, and the crack was reinitiated in the second specimen. Here, it is worth noting that some delay time was required to reinitiate the crack in the second glass specimen after passing through the interface or interlayer. In this work, the shock generating crack type is different; thus, the crack pattern is so complex that we cannot observe a leading single crack throughout the experiments in the first glass specimen. However, from the impedance relation, the transmitted stress energy at the interlayer varies in each specimen, and it reveals different damage patterns in Fig. 10. The yellow color in the figure is the back screen which was used to identify a damage region from the intact region. The yellow

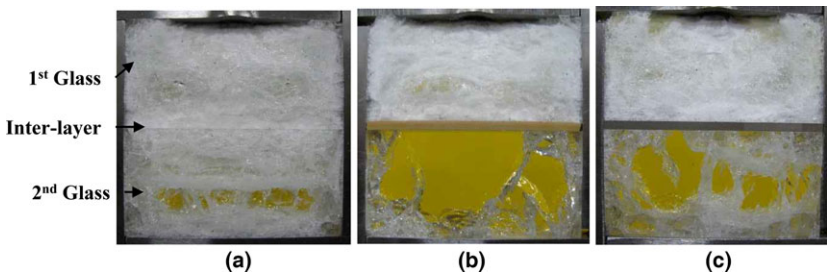

Fig. 10. Damage configurations of recovered specimen. (a) Contact specimen. (b) Layered specimen with rubber interlayer. (c) Layered specimen with stainless steel interlayer.

region is intact region and the white region and lines are damage region and cracks. As the transmitted stress increases, more damage and micro-cracks are observed (Fig. 10a). When the input stress is considerably attenuated, few long cracks are found in the second glass plate (Fig. 10b). Those cracks were generated not from the interlayer but from the interface confined with steel blocks. This means that the cause of the crack generation is tensile stress at the interface (Fig. 6a).

Conclusions

The dynamic impact experiment with an EBW loading technique onto glass laminates has been analyzed for its effectiveness in the study of the dynamic fracture behaviors of glass *in situ*. EBW detonation loads impulse stress onto the specimen of more than 20 GPa and causes shock wave interaction in the specimen without penetration. The initial speeds of a forward progressing fracture and backward fracture are approximately 1.5 km/s, similar to the failure wave and the crack limit speed of glass at high impact stress. The Rayleigh cone angles of damage are observed to be 22° for the confined specimen and 19.5° for the unconfined specimen. The higher the impact stress applied to the specimen, the faster the Rayleigh surface wave propagates, which causes the Rayleigh cone angle to be smaller than the angle with lower impact stress.

Analysis of the energy dissipation and impedance relation at the interlayer reveals that a quantity of <10% of impact energy is transferred to the 2nd glass, and it is matched to the dynamic fracture and the damage pattern of the recovered specimen. The impedance relation at the interlayer plays an important role in transferring stress energy. A low impedance material, as an interlayer, is advantageous to attenuate shock waves more effectively than a relatively high impedance material. The optical density of the shock wave and the fracture shape observed on the high-speed photographs are in good agreement with the impedance relation.

References

1. M. M. Shokrieh, and G. H. Javadpour, "Penetration Analysis of a Projectile in Ceramic Composite Armor," *Comp. Struct.*, 82 269–276 (2008).
2. E. Medvedovski, "Ballistic Performance of Armor Ceramics: Influence of Design and Structure, Part 2," *Ceram. Int.*, 36 2117–2127 (2010).
3. E. Straßburger, "Ballistic Testing of Transparent Armor Ceramics," *J. Eur. Ceram. Soc.*, 29 267–273 (2009).
4. Z. H. Tan, X. Han, W. Zhang, and S. H. Luo, "An Investigation of Failure Mechanism of Ceramic/Metal Armor Subjected to the Impact of Tungsten Projectile," *Int. J. Impact Eng.*, 37 1162–1169 (2010).
5. R. L. Woodward, W. A. Gooch Jr, R. G. W. J. O'Donnell Perciballi, B. J. Baxter, and S. D. Pattie, "A Sturdy of Fragmentation in the Ballistic Impact of Ceramics," *Int. J. Impact Eng.*, 15 605–618 (1994).
6. E. A. Gamble, B. G. Compton, and F. W. Zok, "Impact Response of Layered Steel-Alumina Targets", *Mech. Mater.*, 60, 80–92 (2013).
7. D. A. Shockey, A. H. Marchand, S. R. Skaggs, G. E. Cort, M. W. Burkett, and R. Parker, "Failure Phenomenology of Confined Ceramic Targets and Impact Rods", *Int. J. Impact Eng.*, 9, 263–275 (1990).
8. H. S. Shin, S. N. Chang, and D. K. Kim, "Deformation Behaviors of Zr-Based Bulk Metallic Glass Under Impact Indentation," *Int. J. Mod. Phys. B*, 22 1775–1782 (2008).
9. R. B. Leavy, J. D. Clayton, O. E. Strack, R. M. Brannon, and E. Strassburger, "Edge on Impact Simulation and Experiments," *Procedia Eng.*, 58 445–452 (2013).
10. C. E. Anderson Jr, D. L. Orphal, V. Hohler, M. Moll, and W. Templeton, "Failure and Penetration Response of Borosilicate Glass During Short-Rod Impact," *Int. J. Impact. Eng.*, 36 789–798 (2009).
11. L. C. Forde, W. G. Proud, S. M. Walley, P. D. Curch, and I. G. Cullis, "Ballistic Impact Studies of a Borosilicate Glass," *Int. J. Impact. Eng.*, 37 568–578 (2010).
12. E. Straßburger, and M. Steinhauser, "High speed photographic study of wave propagation and impact damage in transparent laminates", ARL-CR-605, 2008.
13. J. H. Choi, and S. N. Chang, "Fracture Phenomena of Brittle Material against a Shaped Charge Jet," *Int. J. Mod. Phys. B*, 22 1475–1482 (2008).
14. C. D. Jones, J. B. Rioux, and J. W. Locher, "Advances in ballistic performance of commercially available Saint-Gobain sapphire transparent armor composite", Advanced in ceramic armor IV, Ceramic Engineering and Science Proceedings, 29 [6] 63–74, 2008.
15. E. Strassburger, P. Patel, W. McCauley, and D. W. Templeton, "Visualization of wave propagation and impact damage in a polycrystalline transparent ceramic AlON", Proceedings of 22nd International Symposium on Ballistics, Vancouver, Canada, Nov., 2005
16. Soda lime glass (Low-Iron Glass), www.jmcglass.com/down/low.pdf, 2015.
17. RP-87 EBW Detonator, P/N 167-9643, RiSi catalog, 27, 2010.
18. J. E. Kennedy, "Behavior an Utilization of Explosives in Engineering Design," 12th Annual Symposium, ASME, UNIM, Albuquerque, NM, 1972.
19. S. P. Marsh, *LASL Shock Hugoniot Data*, University of California Press, Berkeley, 1980.
20. J. H. Choi, C. H. Lee, and S. N. Chang, "Dynamic fracture phenomena in glass and PMMA", Proceeding of SPIE 21st High speed photography, Daejon, Korea, August 29–September 2, 1994.
21. M. A. Meyers, *Dynamic Behavior of Materials,* John Wiley & Sons, Inc., New York, NY, 1994.
22. E. Straßburger, "Stress wave and damage propagation in transparent laminates at elevated temperatures", U.S. Army Research Laboratory contractor report ACR-CR-639, 2010.
23. J. Kimberley, and K. T. Ramesh, "Visualization of Early Stage Damage Propagation during Hypervelocity Impacts on Brittle Materials," *Procedia Eng.*, 58 678–688 (2013).
24. C. E. Anderson Jr, R. P. Bigger, and C. E. Weiss, "Crack and Damage Velocities in Ballistic Experiments," *Int. J. Appl. Glass Sci.*, 5 374–383 (2014).
25. A. Yavari, and H. Khezrzadeh, "Estimating Terminal Velocity of Rough Cracks in the Framework of Discrete Fractal Fracture Mechanics," *Eng. Fract. Mech.*, 77 1516–1526 (2010).
26. G. I. Kanel, S. V. Razorenov, A. S. Savinykh, A. Rajendran, and Z. Chen, "A Study of the Failure Wave Phenomena in Glasses Composed at Different Levels," *J. Appl. Phys.*, 98 113523 (2005).
27. X. Brajer, P. Forquin, R. Gy, and F. Hild, "The Role of Surface and Volume Defects in the Fracture of Glass under Quasi-Static and Dynamic Loadings," *J. Non-Crys. Solids*, 316 42–53 (2003).

28. F. Abraham, and H. Gao, "How Fast Can Cracks Propagate?" *Phys. Rev. Lett.*, 84 3113–3116 (2000).
29. E. J. Haney, and G. Subhash, "Damage Mechanisms Perspective on Superior Ballistic Performance of Spinel over Sapphire", *Exp. Mech.*, 53 31–46 (2013).
30. H. Senf, and S. Winkler, "Experimental investigation of wave and fracture phenomena in impacted ceramics: Sapphire", ACR-CR-310, Army Research Laboratory, 1997.
31. J. H. Choi, H. J. Lee, C. H. Lee, and D. K. Kim, "Dynamic Fracture Behaviors of Transparent Materials under Detonation Loading", Proceedings of 27th International Symposium on Ballistics, Atlanta, U.S.A., September 22–26, 2014.
32. D. E. Grady, "Analysis of shock and high-rate data for ceramics: Equation of state properties and fragmentation in the ballistic environment", Applied Research Associates, Inc. ARA Project report L 18637, 2009.
33. H. Park, and W. W. Chen, "Experimental Investigation on Dynamic Crack Propagating Perpendicularly through Interface in Glass," *J. Appl. Mech.*, 78 051013 (2011).
34. N. D. Parab, and W. W. Chen, "Crack Propagation through Interfaces in a Borosilicate Glass and Glass Ceramic", *Int. J. Glass Sci.*., 5 353–362 (2014).